

Molecular dynamics simulation of heterogeneous nucleation of bcc-phase at fcc-grainboundary dislocations

Ou, Xiaogin; Sietsma, Jilt; Santofimia, Maria J.

DOI

10.1016/j.scriptamat.2025.117019

Publication date

Document Version Final published version

Published in Scripta Materialia

Citation (APA)

Ou, X., Sietsma, J., & Santofimia, M. J. (2026). Molecular dynamics simulation of heterogeneous nucleation of bcc-phase at fcc-grain-boundary dislocations. *Scripta Materialia*, *271*, Article 117019. https://doi.org/10.1016/j.scriptamat.2025.117019

Important note

To cite this publication, please use the final published version (if applicable). Please check the document version above.

Copyright

Other than for strictly personal use, it is not permitted to download, forward or distribute the text or part of it, without the consent of the author(s) and/or copyright holder(s), unless the work is under an open content license such as Creative Commons.

Please contact us and provide details if you believe this document breaches copyrights. We will remove access to the work immediately and investigate your claim.

ELSEVIER

Contents lists available at ScienceDirect

Scripta Materialia

journal homepage: www.journals.elsevier.com/scripta-materialia



Molecular dynamics simulation of heterogeneous nucleation of bcc-phase at fcc-grain-boundary dislocations

Xiaoqin Ou^{a,b,*}, Jilt Sietsma^a, Maria J. Santofimia^a

- a Department Materials Science and Engineering, Delft University of Technology, Mekelweg 2, 2628CD, Delft, the Netherlands
- ^b State Key Laboratory of Powder Metallurgy, Central South University, Changsha 410083, China

ARTICLE INFO

Keywords:
Molecular dynamics
Thermodynamics
Heterogeneous nucleation of phase
transformations
Dislocation
Austenite-to-ferrite phase transformation

ABSTRACT

Nucleation during phase transformations plays an important role in the crystal structure, the grain size and the texture of the forming product phase, and thus determines the properties of the obtained material. In this study, molecular dynamics simulation is employed to study the heterogeneous nucleation of bcc-phase in fcc iron. It is found that the bcc-phase nucleates at the dislocations in the fcc/fcc grain boundaries in a pseudo-cylindrical morphology. The energy change as a function of the bcc nucleus size conforms to the Cahn's classical model with no energy barrier, and provides interface energies and elastic constants comparable to theoretical calculations and experimental data. Nevertheless, there are aspects that cannot be explained by the classical Cahn nucleation theory, namely the stepwise "fcc-intermediate-bcc" nucleation process, and the aggregation of discrete subnuclei. This noclassical nucleation processes contribute to the decrease of energy barrier and the stabilization of the bcc nucleus

Main text

Nucleation and growth of a phase in alloys control the microstructural evolution, which thereby determine the properties of alloys [1,2]. Identifying the nucleation mechanisms is a long-standing problem, especially in polycrystalline materials such as metals and ceramics, because it is difficult for experiments to monitor the formation of very small nuclei at very short time frames in the bulk of materials [2].

The technological importance of steel has induced extensive studies of phase transformations. Ferrite nucleation (body center cubic – bcc) from austenite (face center cubic – fcc) in steels has been experimentally studied [2–7] based on the classical nucleation theory (CNT) [8]. According to the CNT [8], nucleation of a new phase needs to overcome an energy barrier for the subsequent growth. However, discrepancies arose between those studies [2,3,5,7,8], for example, regarding the critical nucleus size of the ferrite. Offerman et al. [2] concluded a critical nucleus size of 10-100 atoms while Aaronson et al. [5] estimated it of about 320 atoms. This discrepancy arises from the indirect estimation of the critical size from experiments, in which the growth of existing ferrite grains has already occur.

The identification of nonclassical nucleation pathways, which facilitate stabilisation of nuclei by circumventing the high energy barrier

predicted by the CNT, has been one of the most important insights in recent work both by simulations [9-13] and experiments [4,14-19]. Ou et al. [13] studied the thermodynamics of the homogeneous nucleation of bcc from fcc in Fe by molecular dynamics (MD) simulations based on the CNT and gave a critical nucleus of 95 \pm 20 atoms with a one-dimensional size of about 10 Å. However, the CNT overestimated the energy barrier for the homogeneous nucleation due to the occurrence of nonclassical nucleation by the aggregation of neighbouring nuclei and the formation of an intermediate state between the fcc and bcc-phases [13]. These nonclassical nucleation pathways were also observed experimentally during the nucleation process in diverse systems, such as colloidal particles [4,14], small molecules [15,16] and metallic systems [17,18]. Specifically, a recent study by Hutchinson and Brechet [19] reported the limitation of the CNT in predicting solid-state nucleation at low temperatures and proposed a new and complementary "geometric cluster" model for phase nucleation during crystallization in metallic systems with low atomic mobility. Heterogeneous nucleation at defects is more favoured than homogeneous nucleation [20]. Grain boundaries in the parent phase are eliminated during the nucleation of the new phase, leading to the reduction of the energy barrier for nucleation [21]. Specifically, dislocations at grain boundaries can act as sites for nucleation [22]. Cahn [23] proposed a theoretical model to

^{*} Corresponding author at: State Key Laboratory of Powder Metallurgy, Central South University, Changsha 410083, China. E-mail address: Xiaoqin.Ouyang@csu.edu.cn (X. Ou).

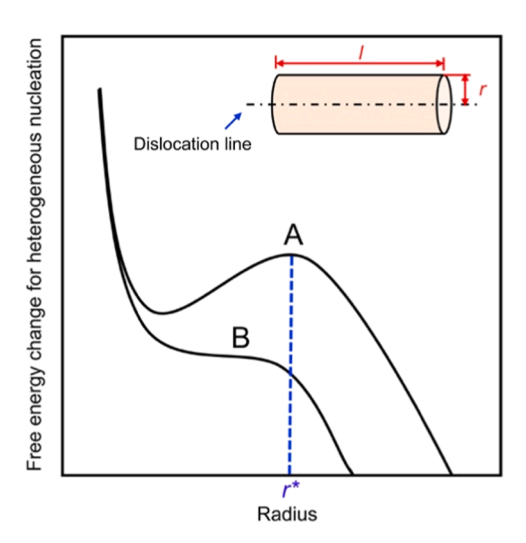


Fig. 1. Free-energy change per unit length of a cylindrical nucleus forming at a dislocation. No local maximum exists with α greater than 1 (Curve B). A similar figure can be found in Reference [23]. The insert shows the nucleus with a cylindrical morphology, r and l represent the radius and the length of the nucleus, $r \ll l$.

Table 1 Information regarding the two simulation systems considered in this work: System A is represented in supplementary figure A1 (a) and System B in supplementary figure A1 (b).

	System A	System B
Lattice parameter for the fcc	3.658 Å	3.658 Å
Total number of atoms	443,520	669,456
Box size (Å ³)	161.52 × 146.32 × 230.21	286.75 × 124.16 × 230.55

describe the thermodynamic features for nucleation at dislocations. In that model, the nucleus is assumed to be a cylinder lying along the core of the dislocation with a circular cross-section perpendicular to the dislocation line, as indicated in Fig. 1. The free-energy change ΔG due to the formation of the nucleus per unit length can be divided into three terms:

- (a) the strain-energy term (the distortion energy stored in the dislocations), $A \ln \left(\frac{r}{r_0} \right)$;
- (b) the volume free-energy term (the energy difference between the parent and product phase), $\pi\Delta g_V r^2$;
- (c) the surface free-energy term (the energy required for creation of new phase interfaces), $2\pi\gamma r$.

In these expressions A is equal to $\frac{\mu b^2}{4\pi(1-\nu)}$ for edge dislocations and to $\frac{\mu b^2}{4\pi}$ for screw dislocations; μ is the elastic shear modulus, b is the length of Burgers vector and ν is the Poisson ratio. r_0 is an effective parameter taking into account both the core radius r_c and the core energy of a dislocation $G_c = A \ln \left(\frac{r_c}{r_0}\right)$. r is the radius of the nucleus, γ is the interface energy, and Δg_V is the volume free-energy difference between the parent and product phases per unit of volume.

In this approach, the planar faces of the cylinder are neglected. Therefore, the free-energy change ΔG of the nucleus per unit length is expressed as:

$$\Delta G = -A \ln \frac{r}{r_0} - \pi \Delta g_V r^2 + 2\pi \gamma r \tag{1}$$

When the parameter $\alpha=\frac{2A\Delta g_V}{\pi\gamma^2}$ is less than 1, a local maximum ΔG^* in $\Delta G(r)$ exists at a value of

$$r^* = \frac{\gamma}{2\Delta g_V} \left(1 + \sqrt{1 - \frac{2A\Delta g_V}{\pi \gamma^2}} \right) \tag{2}$$

$$\Delta G^* = -A \ln \left[\frac{\gamma}{2\Delta g_V r_0} \left(1 + \sqrt{1 - \frac{2A\Delta g_V}{\pi \gamma^2}} \right) \right]$$

$$+ \frac{\pi \gamma^2}{2\Delta g_V} \left(1 + 2\sqrt{1 - \frac{2A\Delta g_V}{\pi \gamma^2}} \right) + \frac{A}{2}$$
(3)

This corresponds to Curve A in Fig. 1. No local maximum of ΔG exists when $\alpha > 1$ (Curve B in Fig. 1). For the details of the thermodynamic analysis, please refer to the supplementary material.

The present work considers the classical Cahn nucleation model in studying the thermodynamics of heterogeneous nucleation of bcc-phase at dislocations in fcc/fcc grain boundaries in iron by MD simulations. The overall aim is to better understand the nature of heterogeneous nucleation during solid-solid phase transformations in metals. Nonclassical nucleation mechanisms are also considered.

In this study, two simulation systems with fcc/fcc grain boundaries in pure iron are studied: System A includes two low-angle grain boundaries (LAGB) composed of an array of edge dislocations with the Burgers vectors $b_{LAGB} = \frac{1}{2}\langle 101 \rangle_{fcc}$; System B includes two {111} twin boundaries, one is a coherent twin grain boundary (CTGB) and the other is a semi-coherent twin grain boundary (STGB) involving 5.7° rotation around the $[1\overline{10}]_{fcc}$ direction from the $(111)_{fcc}$ twinning plane (see Table 1, Fig. 2 and supplementary figure A1). Both systems are relaxed and isothermally treated at 100 K in LAMMPS [24]. For details of the simulations, please refer to the supplementary materials.

Fig. 2 shows the bcc nuclei on the LAGB at different simulation times. Edge dislocations, indicated by the unidentified atoms in Fig. 2(a), appear periodically at the fcc/fcc grain boundaries and act as heterogeneous nucleation sites. The enlarged views of the regions inside the red rectangle in Fig. 2(b) illustrate the nucleation process. Fig. 2(c) shows atoms that are not in the fcc structure. An individual bcc nucleus forms at the core of each dislocation extending along the dislocation line. These nuclei impinge during the subsequent growth into the fcc parent grains after 500 fs. Note that after 250 fs some of the atoms that initially were in an unidentified structure have been relaxed to the fcc structure.

Fig. 3 shows the configurations of the bcc-phase at the STGB in System B at different simulation times. The enlarged view of the area marked by the red rectangle is included in the insert in Fig. 3(a). No nucleation takes place at the CTGB, which parallels the $\{111\}_{fcc}$ plane and exhibits an hcp structure. The STGB is 5.7° rotated from the $(111)_{fcc}$ plane, leading to the alternating appearance of coherent (hcp structure) and incoherent (unidentified structure) regions at the grain boundary. The nucleation of bcc initiates from the incoherent part along the dislocation line at the STGB (Fig. 3(b)). The bcc nuclei are therefore separated by the coherent parts. Every single bcc nucleus is exempted from the influence of its neighbouring nucleus during the time range considered in the present study. The neighbouring bcc nuclei overlap after 1500 fs. The bcc nuclei grow in multiple directions by consuming the two fcc parent grains and the STGB.

Figs. 4(a) and (b) show the evolution of the dislocations at the LAGB and STGB, respectively. From Fig. 4(a), the dislocations present at the LAGB mainly have the Burgers vector $\frac{1}{2}\langle 110\rangle_{fcc}$ and are nearly parallel to the y axis in the first 200 fs. After that, the parallel dislocation lines are interrupted due to the bcc nucleation at the LAGB. The dislocation lines become discontinuous with the growth of bcc and disappear after around 600 fs. At the STGB in Fig. 4(b), there are mainly Shockley partial dislocations with the Burgers vector $\frac{1}{6}\langle 112\rangle_{fcc}$. Rather than

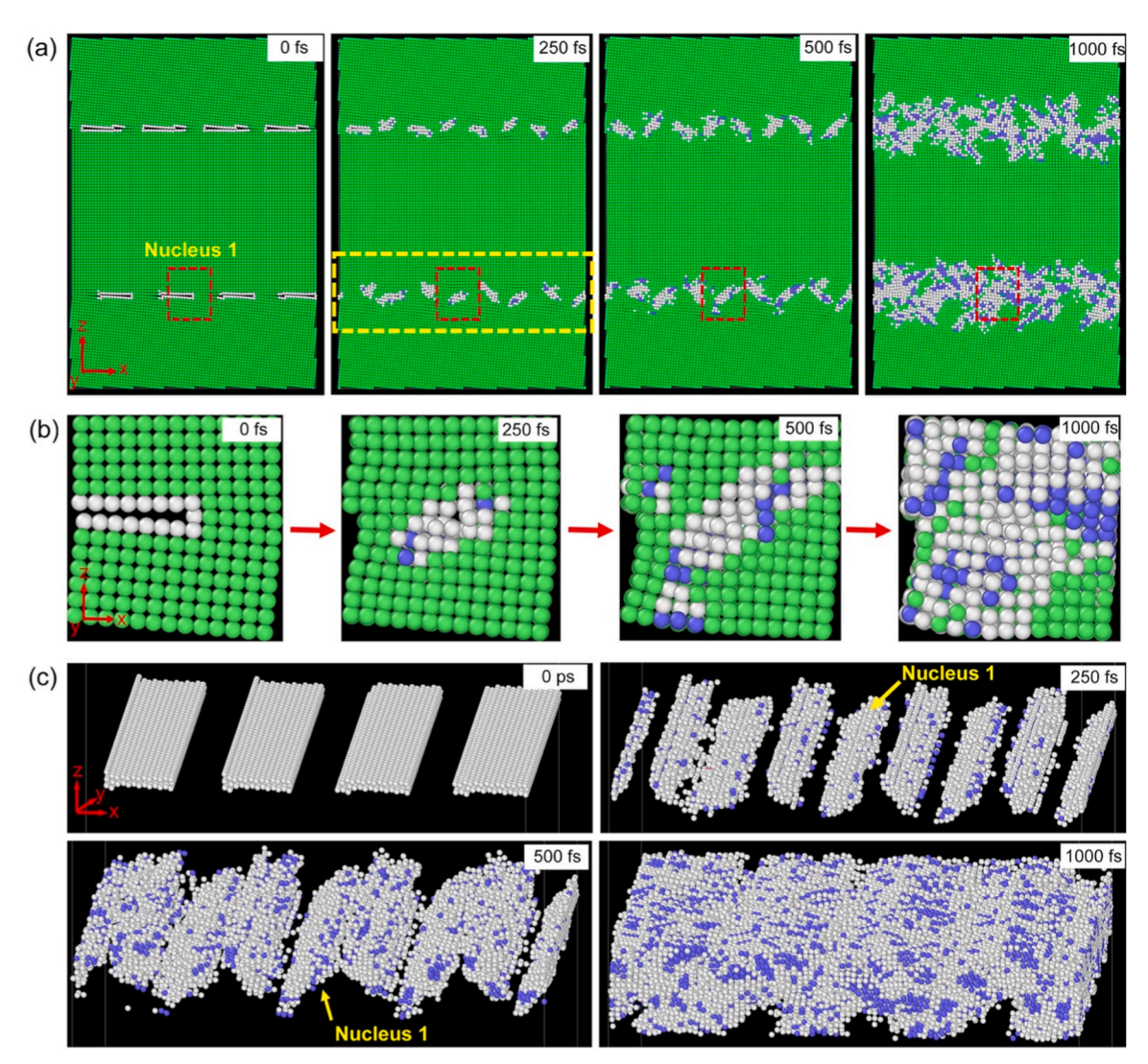


Fig. 2. (a) Time evolution of the bcc nucleation at the edge dislocations at the LAGB at 0 fs, 250 fs, 500 fs and 1000 fs; (b) Enlarged view of the regions marked by the red dashed rectangle in figure (a); (c) Time evolution of the bcc nucleation at the LAGB 2, as marked by the yellow dashed rectangle in figure (a), the fcc atoms are not shown. Colours of atoms represent different phase structures: blue-bcc; green-fcc; red-hcp; white-unidentified.

straight, the dislocation lines at the STGB are curved and intersect at multiple locations. Similar to the LAGB, dislocations vanish as the nucleation and growth of bcc at the STGB progress. Nearly no dislocations are detected after 1000 fs.

Two bcc nuclei, namely Nucleus 1 and Nucleus 2, are included in the selected volumes marked by the red rectangle in Figs. 2 and 3, respectively. Table 1 indicates the number of atoms in the selected volumes. Figs. 5(a) and (b) show the relationship between the energy change ΔG and the effective radius r of Nucleus 1 and 2, respectively. The red curves are fitted to the thermodynamic data of Nucleus 1 and 2 according to the classical Cahn nucleation model in Eq. (1), with the values of the fitting parameters in Table 2. The energy change as a function of the radius for both nuclei agrees well with Cahn's model, which corresponds to a shape described as "B" in Fig. 1. The parameter α for both nuclei is greater than 1, which means that no activation energy is involved in the bcc nucleation at the dislocations in the LAGB and STGB. In such cases, the sum of the removed strain energy and the volume energy change due to the formation of the bcc nucleus surpass the interface energy [23]. Similar results are obtained for a second nucleus in each system, Nucleus 1' and Nucleus 2', as indicated by the fitting parameters in Table 2 and supplementary figure A2.

The elastic shear modulus μ and Poisson's ratio ν for cubic structures are related to the elastic constants C_{ij} through [25]:

$$\mu = \frac{C_{11} - C_{12} + 3C_{44}}{5} \tag{4}$$

$$\nu = \frac{C_{11} + 4C_{12} - 2C_{44}}{2(2C_{11} + 3C_{12} + C_{44})} \tag{5}$$

For the fcc Fe crystal, the elastic constants C_{ij} at different temperatures from either theoretical calculations or experiments [26–31] are included in Table 3. By substituting the elastic constants into Eq. (4) and (5), the corresponding shear modulus μ , Poisson's ratio ν and thus the coefficient A are calculated (Table 3). A ranges between 1×10^{-10} J/m and 7×10^{-10} J/m, which is comparable to the fitted coefficient for the nuclei in System A in Table 2. The fitted coefficient A for the nuclei in System B is larger than for System A and equals to 16×10^{-10} J/m. This may result from the complex dislocations existing at the STGB.

Experimental data suggests about 800 mJ/m² for the bcc/fcc interface energy, which is an average of values obtained for incoherent, semicoherent and coherent interfaces [32]. Peng *et al.* [4] reported that the incoherent interface energy in metals ranges from 500 to 1000 mJ/m², for semi-coherent interfaces from 200 to 500 mJ/m² and for coherent interfaces below 200 mJ/m². Based on the MD simulations [33], the present authors calculated the interface energies to be 530 mJ/m² and 686 mJ/m² for the semi-coherent bcc/fcc interfaces in the

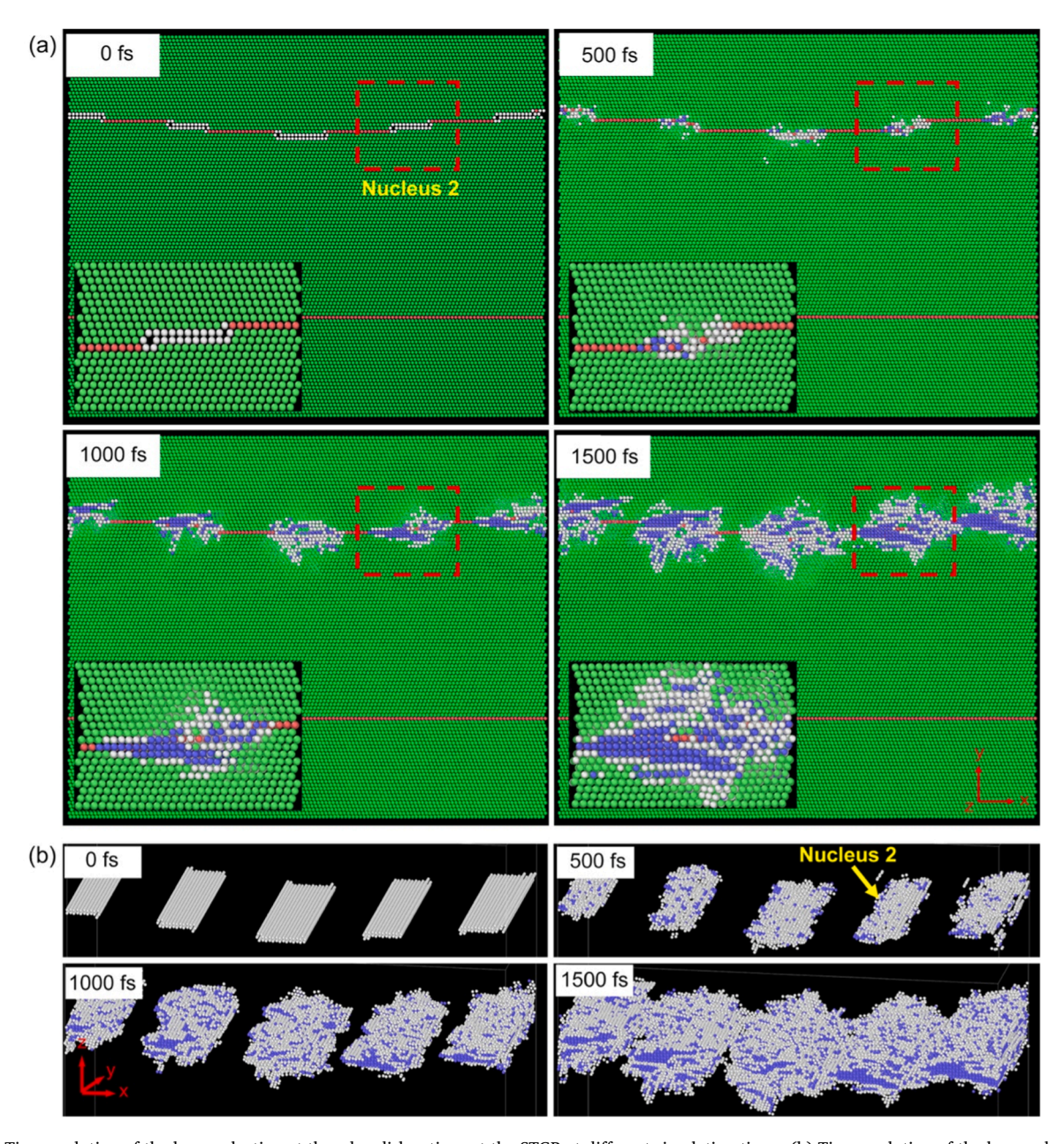


Fig. 3. (a) Time evolution of the bcc nucleation at the edge dislocations at the STGB at different simulation times; (b) Time evolution of the bcc nucleation at the STGB, the fcc atoms are not shown. The inserts in figure (a) are the enlarged view of the corresponding area marked by the red dashed rectangle. Colours of atoms represent different phase structures: blue-bcc; green-fcc; red-hcp; white-unidentified.

X. Ou et al. Scripta Materialia 271 (2026) 117019

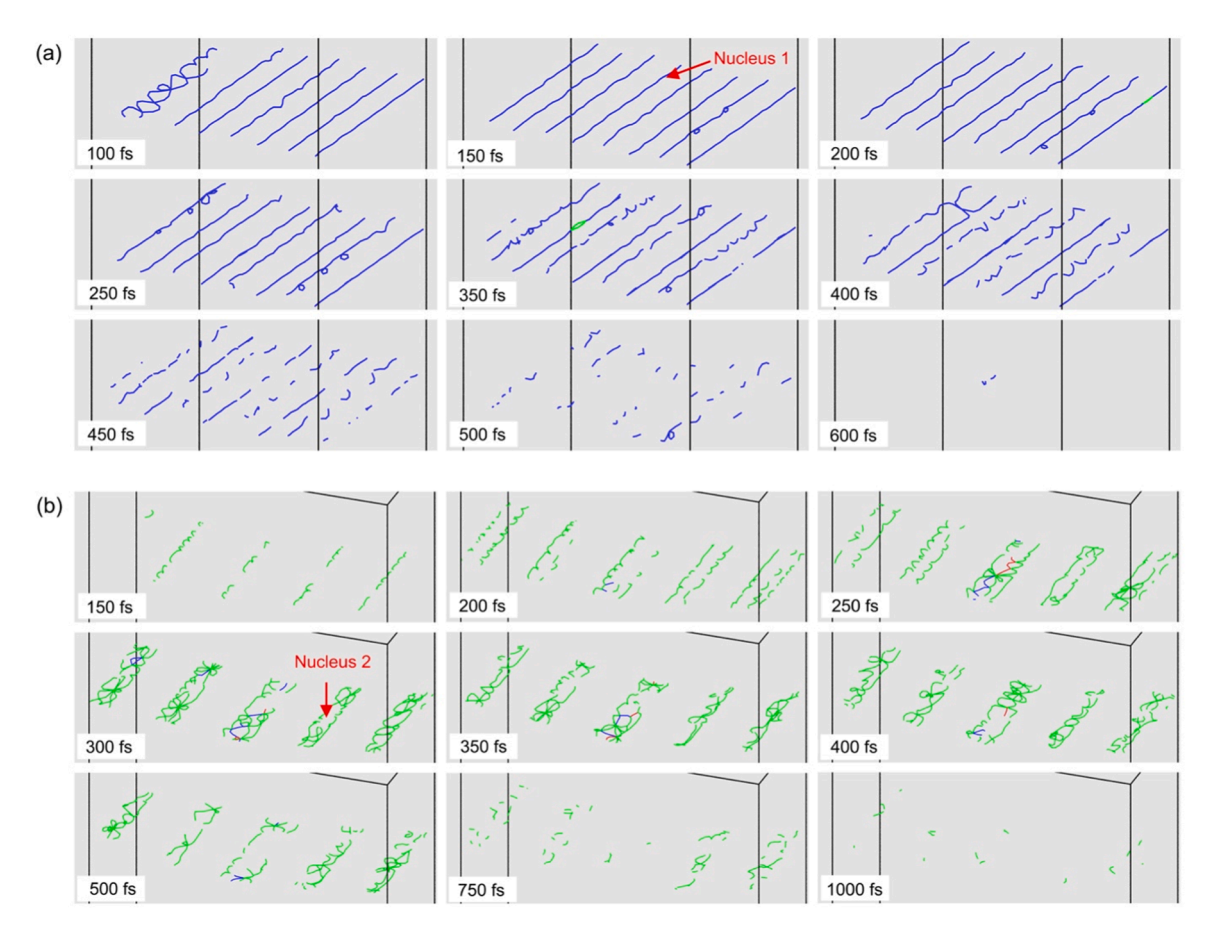


Fig. 4. Time evolution of the dislocation lines at: (a) LAGB 2, (b) STGB, respectively. Colours of the dislocation lines represent different dislocation types, with Burgers vector: blue $-\frac{1}{2}\langle 110\rangle$; green $-\frac{1}{6}\langle 112\rangle$; red – other.

Nishiyama-Wassermann (NW) [34] and Kurdjumov-Sachs (KS) [35] orientation relationship (OR), respectively. Thus, from Table 2, the interface energy 567 mJ/m 2 for Nucleus 1 indicates a semi-coherent interface, while 1031 mJ/m 2 indicates an incoherent bcc/fcc interface for Nucleus 2.

Besides, the radius of the dislocation core r_c can be approximated to two times the length of a Burgers vector [36]. For the lattice parameter $a_{\rm fcc}=3.658$ Å, the shortest length of Burgers vector $b=\frac{1}{2}\langle 1\ 1\ 0\rangle_{\rm fcc}$ is 2.587 Å. According to Eq. (1), the core energy G_c ranges between 7×10^{-10} J/m and 16×10^{-10} J/m, which is of the same magnitude as the fitting values of A for Nucleus 1 and Nucleus 2 in Table 2.

The bcc nuclei consist of a bcc-structured core and a shell composed of unidentified atoms (Figs. 2 and 3, figures A3 and A4). Generally, the phase/grain boundary consists of one (or two) atomic layers with structural disorder. The unidentified atoms between the bcc core and fcc phase, however, extend over a distinctly broader range of atomic layers (4 or more layers) than a normal monolayer between the parent and product lattices [37]. Thus, those unidentified atoms with structural disorder not only act as the phase interface but also as an amorphous intermediate phase between the fcc and bcc structures. The formation of such an intermediate phase during the nucleation process was also observed previously in other materials [17,37–39].

Figs. 5(c) and (d) show the time evolution of the number of atoms with different structures for Nucleus 1 and 2. The number of atoms in the bcc and unidentified structure shows an increasing trend with time, indicating that the fcc-phase transforms partly to the bcc-phase and partly to the intermediate state. Furthermore, the number of atoms in the intermediate state is higher than that in the bcc structure during the nucleation process. Fig. 5(e) and (f) show that the energy change ΔG of individual nucleus mainly results from the unidentified atoms, with

minor effects from the bcc atoms, especially in the initial nucleation stage. The energy change of the unidentified atoms (or the intermediate state) decreases with time, while that of the bcc exhibits an energy barrier during the nucleation process (inserts in Fig. 5(e) and (f)).

Nonclassical pathways occur during the bcc nucleation in fcc iron in the present study. The fcc-phase transforms firstly to an amorphous intermediate state, the nucleation of which initiates from the dislocations and follows the classical Cahn's model with no energy barriers. Then, the bcc-phase nucleates either from the intermediate state or from the fcc-phase. The energy barrier exists for the stabilization of each nucleus (inserts in Fig. 5(e) and (f)). Besides, multiple discrete bcc subnuclei forming along the dislocation line are bound by the intermediate state as a continuous aggregate. The bcc subnuclei located on opposite sides of the dislocation (yellow mark) evolve in the NW and KS OR, respectively (figure A5(c,d), figure A6(c,d)). These nonclassical pathways, namely stepwise nucleation and aggregation of subnuclei, have been observed previously in diverse materials [4,13-19,37-39]. During the prenucleation period of the synthesis of nanoparticles in metals such as gold [17,38,39] and CdSe [40], the formation of an amorphous intermediate phase (or nanoclusters) reveals the presence of local minima in the energy landscape and lowers the energy barrier for nucleation with respect to the one predicted by the CNT [16]. While the stepwise nucleation involves thermodynamic stabilization via structural change, the role of aggregation in stabilising nuclei correlates to kinetic origin by abruptly increasing nucleus size and "tunneling" through the high energy barrier of the CNT [16,18]. Evidence by high resolution electron tomography reveals multiple crystal domains in a single platinum nanoparticle, which originate from the aggregation of smaller nanoclusters during the prenucleation period of the nanoparticle formation process [18].

In summary, this paper performs a thermodynamic analysis of

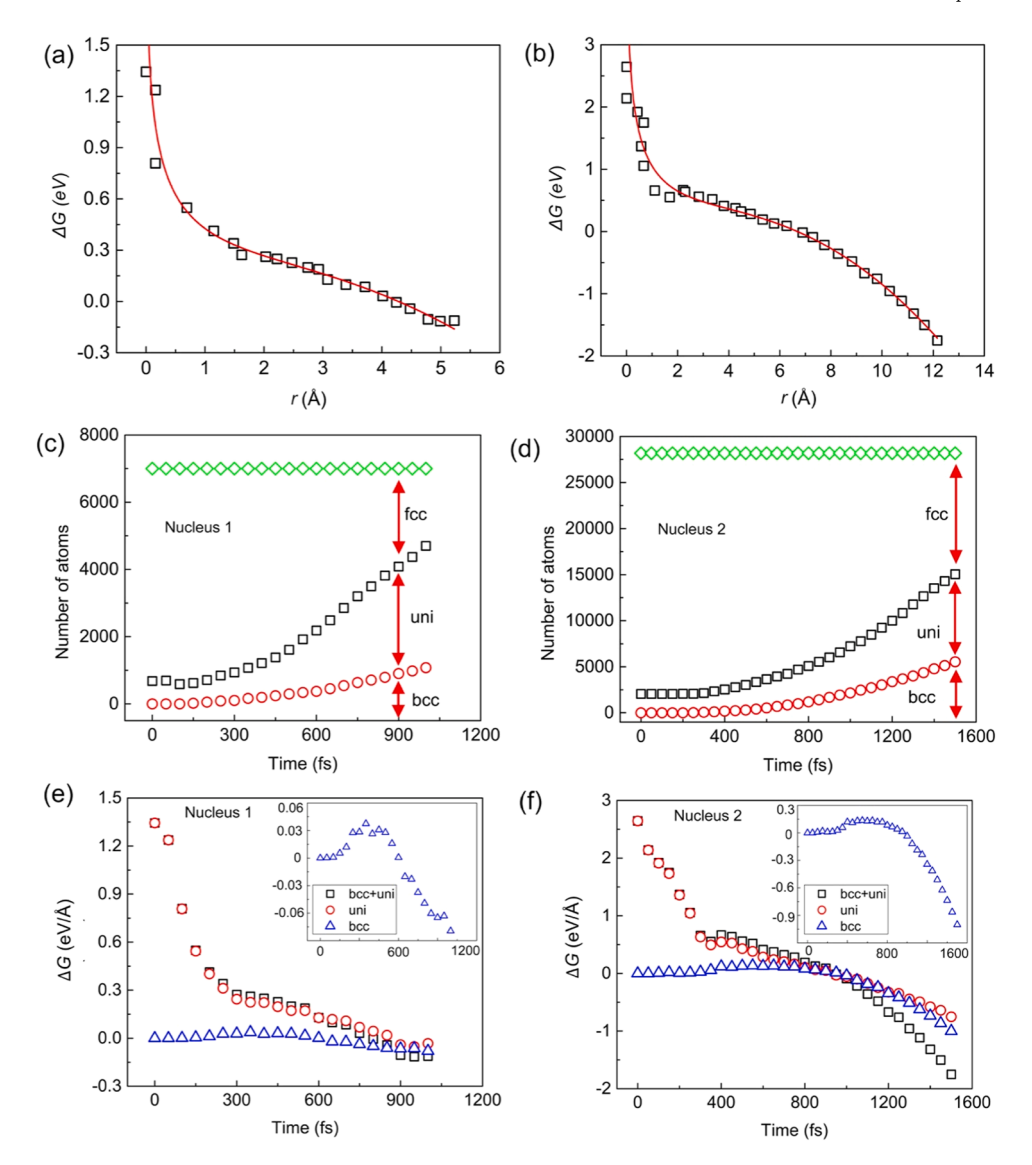


Fig. 5. The relation between the energy change ΔG per unit length along the core of the dislocation and radius r of the nuclei: (a) Nucleus 1 and (b) Nucleus 2. The black open dots in (a, b) are the MD data. The red curves are fitted according to Eq. (1). (c, d) Time evolution of the number of atoms with different structures in the selected volume for Nucleus 1 and Nucleus 2, respectively; (e, f) Contribution of the bcc (triangles) and unidentified atoms (circles) to the free-energy change ΔG (squares) of the bcc Nucleus 1 and Nucleus 2, respectively. The inserts in (e) and (f) show the enlarged view for the energy change of the bcc atoms during nucleation.

Table 2 The fitting parameters of the curves for the nuclei in two systems in Fig. 5 and supplementary figure A2 according to Eq. (1). n_0 represent the number of atoms in the selected volume for individual nucleus, as shown in Fig. 2b and 3a, respectively.

Nucleus	n_0	A (10 ⁻¹⁰ J/m)	Δu_V (meV/ $\mathring{\mathrm{A}}^3$)	γ (mJ/ m ²)	r ₀ (Å)	G _c (10 ⁻¹⁰ J/m)	α
1	7000	7	10.23	567	1.8	7	2.1
1'	7600	8	10.23	663	1.6	9	2.0
2	26,928	16	10.23	1031	1.9	16	1.6
2'	28,171	16	10.23	941	3.1	8	1.9

heterogeneous nucleation by MD simulations. Two fcc/fcc grain boundaries are studied: a low-angle grain boundary and a semi-coherent twinning boundary. Heterogeneous nucleation of the bcc-phase occurs at the dislocations on both fcc/fcc grain boundaries. The energy change of the nucleus as a function of the nucleus size conforms to the classical Cahn's nucleation theory in absence of energy barrier. The estimated

Table 3 The elastic constants, shear modulus and Poisson's ratio for fcc Fe from References [26–31]. μ , ν and parameter A are calculated and included.

Reference	T (K)	C ₁₁ (GPa)	C ₁₂ (GPa)	C ₄₄ (GPa)	μ (GPa)	ν	A (10 ⁻¹⁰ J/m)
[26,27]	0	67	40	10	11.4	0.39	1
[31]	298	230	135	117	89.2	0.27	7
[28]	1428	154	122	77	52.6	0.32	4
[29]	1428	154	143.9	78.4	49.1	0.35	4
[30]	1428	181	156	83.3	55.0	0.35	5

By assuming the lattice parameter $a=3.658\,\mathrm{\AA}$, the square of the Burgers vector $b^2=6.69\,\mathrm{\AA}^2$.

elastic constants and interface energies are comparable to published values.

However, simulations show aspects that are not considered by the classical Cahn's nucleation theory. The fcc-phase transforms to an intermediate state before the nucleation of the bcc-phase. The

intermediate state initiates from the dislocations without energy barrier. This is followed/accompanied by the nucleation of the bcc-phase from the intermediate state or from the fcc-phase, where a nucleation energy barrier is involved. The bcc-nuclei are aggregates of discrete subnuclei, which are bound by the intermediate state. Such neighbouring subnuclei may have different crystallographic orientations.

CRediT authorship contribution statement

Xiaoqin Ou: Writing – original draft, Visualization, Validation, Project administration, Methodology, Investigation, Funding acquisition, Formal analysis, Data curation. Jilt Sietsma: Writing – review & editing, Validation, Supervision, Project administration, Methodology, Investigation, Funding acquisition, Data curation, Conceptualization. Maria J. Santofimia: Writing – review & editing, Visualization, Validation, Supervision, Project administration, Methodology, Investigation, Funding acquisition, Data curation, Conceptualization.

Declaration of competing interest

The authors declare that they have no known competing financial interests or personal relationships that could have appeared to influence the work reported in this paper.

Acknowledgements

Funding: This work was supported by the European Research Council under the European Union's Seventh Framework Programme FP7/2007-2013/ERC [grant agreement n° 306292], National Natural Science Foundation of China [grant number 51901248] and Natural Science Foundation of Hunan Province [grant number 2023JJ40742], the High-Performance Computing Center of Central South University.

Supplementary materials

Supplementary material associated with this article can be found, in the online version, at doi:10.1016/j.scriptamat.2025.117019.

References

- [1] L. Zhang, W.Q. Ren, A. Samanta, Q. Du, Recent developments in computational modelling of nucleation in phase transformations, npj Comput. Mater. 2 (2016) 16003.
- [2] S.E. Offerman, N.H. van Dijk, J. Sietsma, S. Grigull, E.M. Lauridsen, L. Margulies, H.F. Poulsen, M. Th. Rekveldt, S. van der Zwaag, Grain nucleation and growth during phase transformations, Science 298 (2002) 1003–1005.
- [3] N.H. Van Dijk, S.E. Offerman, J. Sietsma, S. Van der Zwaag, Barrier-free heterogeneous grain nucleation in polycrystalline materials: the austenite to ferrite phase transformation in steel, Acta Mater. 55 (2007) 4489–4498.
- [4] Y. Peng, W. Feng, Z.R. Wang, A.M. Alsayed, Z.X. Zhang, A.G. Yodh, Y.L. Han, Two-step nucleation mechanism in solid-solid phase transitions, Nat. Mater. 14 (2015) 101–108.
- [5] H.I. Aaronson, W.F. Lange III, G.R. Purdy, Discussion to "Grain nucleation and growth during phase transformations" by S.E. Offerman et al., Science, 298, 1003 (November 1, 2002), Scripta Mater. 51 (2004) 931–935.
- [6] W.F. Lange III, M.E. Enomoto, H.I. Aaronson, The kinetics of ferrite nucleation at austenite grain boundaries in Fe-C alloys, Metall. Trans. A 19 (1988) 427–440.
- [7] S.E. Offerman, N.H. van Dijk, J. Sietsma, S. van der Zwaag, E.M. Lauridsen, L. Margulies, S. Grigull, H.F. Poulsen, Reply to the discussion by Aaronson et al. to "Grain nucleation and growth during phase transformations" by S.E. Offerman et al., Science, 298, 1003 (November 1, 2002), Scripta Mater. 51 (2004) 937–941.
- [8] J.W. Christian, The Theory of Transformations in Metals and Alloys, Pergamon, Oxford, 1981.

- [9] H. Song, J.J. Hoyt, An atomistic simulation study of the migration of an austeniteferrite interface in pure Fe, Acta Mater. 61 (2013) 1189–1196.
- [10] B.J. Wang, H.M. Urbassek, Phase transitions in an Fe system containing a bcc/fcc phase boundary: an atomistic study, Phys. Rev. B 87 (2013) 104108.
- [11] X.S. Yang, S. Sun, T.Y. Zhang, The mechanism of bcc α' nucleation in single hcp ε laths in the fcc γ → hcp ε → bcc α' martensitic phase transformation, Acta Mater. 95 (2015) 264–273.
- [12] S.Y. Hu, M.I. Baskes, M. Stan, L.Q. Chen, Atomistic calculations of interfacial energies, nucleus shape and size of 6' precipitates in Al-Cu alloys, Acta Mater. 54 (2006) 4699–4707.
- [13] X. Ou, J. Sietsma, M.J. Santofimia, Fundamental study of nonclassical nucleation mechanisms in iron, Acta Mater. 226 (2022) 117655.
- [14] Z. Ou, Z. Wang, B. Luo, E. Luijten, Q. Chen, Kinetic pathways of crystallization at the nanoscale, Nat. Mater. 19 (2020) 450–455.
- [15] M.H. Nielsen, S. Aloni, J.J. De Yoreo, In situ TEM imaging of CaCO₃ nucleation reveals coexistence of direct and indirect pathways, Science 345 (2014) 1158–1162
- [16] J. Lee, J. Yang, S.G. Kwon, T. Hyeon, Nonclassical nucleation and growth of inorganic nanoparticles, Nat. Rev. Mater. 1 (2016) 16034.
- [17] S. Jeon, T. Heo, S.-Y. Hwang, J. Ciston, K.C. Bustillo, B.W. Reed, J. Ham, S. Kang, S. Kim, J. Lim, K. Lim, J.S. Kim, M.-H. Kang, R.S. Bloom, S. Hong, K. Kim, A. Zettl, W.Y. Kim, P. Ercius, J. Park, W.C. Lee, Reversible disorder-order transitions in atomic crystal nucleation, Science 371 (2021) 498–503.
- [18] J. Park, H. Elmlund, P. Ercius, J.M. Yuk, D.T. Limmer, Q. Chen, K. Kim, S.H. Han, D.A. Weitz, A. Zettl, P. A, Alivisatos, 3D structure of individual nanocrystals in solution by electron microscopy, Science 349 (2015) 290–295.
- [19] C. Hutchinson, Y. Brechet, A new approach to solid-state nucleation in kineticallyconstrained systems, Acta Mater. 283 (2025) 120521.
- [20] P.J. Clemm, Fisher J.C, The influence of grain boundaries on the nucleation of secondary phases, Acta Metall 3 (1955) 70–71.
- [21] H. Sharma, J. Sietsma, S.E. Offerman, Preferential nucleation during polymorphic transformations, Sci. Rep. 6 (2016) 30860.
- [22] C.C. Dollins, Nucleation on dislocations, Acta Metall. 18 (1970) 1209-1215.
- [23] J.W. Cahn, Nucleation on dislocations, Acta Metall. 5 (1957) 169-172.
- [24] S. Plimpton, Fast parallel algorithms for short-range molecular dynamics, J. Comp. Phys. 117 (1995) 1–19. http://lammps.sandia.gov/. Accessed on September 26th, 2025.
- [25] G. Ghosh, G.B. Olson, The isotropic shear modulus of multi-component Fe-base solid solutions, Acta Mater. 50 (2002) 2655–2675.
- [26] M.I. Mendelev, S. Han, D.J. Srolovitz, Development of new interatomic potentials appropriate for crystalline and liquid iron, Phil. Mag. 83 (2003) 3977–3994.
- [27] M. Müller, P. Erhart, K. Albe, Analytic bond-order potential for bcc and fcc iron-comparison with established embedded-atom method potentials, J. Phys.: Condens. Matter. 19 (2007) 326220.
- [28] J. Zaretsky, C. Stasis, Lattice dynamics of γ-Fe, Phys. Rev. B 35 (1987) 4500–4502.
- [29] F. Gao, R.L. Johnston, J.N. Murrell, Empirical many-body potential energy functions for iron, Phys. Chem. 97 (1993) 12073–12082.
- [30] N. Singh, Lattice Dynamics of γ-Iron at 1428 K, Phys. Stat. Sol. B 156 (1989) K33–K36.
- [31] E.A. Brandes, G.B. Brook, Smithells Metals Reference Handbook, Butterworth-Heinemann, Oxford, 1992 seventh ed.
- [32] Z. Yang, R.A. Johnson, An EAM simulation of the alpha-gamma iron interface, Modell. Simul. Mater. Sci. Eng. 1 (1993) 707–716.
- [33] X. Ou, J. Sietsma, M.J. Santofimia, Molecular dynamics simulations of the mechanisms controlling the propagation of bcc/fcc semi-coherent interfaces in iron, Modelling Simul. Mater. Sci. Eng. 24 (2016) 055019.
- [34] Z. Nishiyama, X-ray investigation of the mechanism of the transformation from face-centred to body-centred cubic lattice, Sci. Rep. Tohoku Imp. Univ. 23 (1934) 637–664.
- [35] G.V. Kurdjumov, G. Sachs, About the mechanism of steel hardening, Z. Phys. 64 (1930) 325–343.
- [36] D. Hull, D.J. Bacon, Introduction to dislocations, fifth ed.. Butterworth-Heinemann, Oxford, 2011.
- [37] W. Qi, Y. Peng, Y. Han, R.K. Bowles, M. Dijkstra, Nonclassical nucleation in a solidsolid transition of confined hard spheres, Phys. Rev. Lett. 115 (2015) 85701.
- [38] N.D. Loh, S. Sen, M. Bosman, S.F. Tan, J. Zhong, C.A. Nijhuis, P. Král, P. Matsudaira, U. Mirsaidov, Multistep nucleation of nanocrystals in aqueous solution, Nat. Chem. 9 (2017) 77–82.
- [39] I.L. Garzón, A. Posada-Amarillas, Structural and vibrational analysis of amorphous Au55 clusters, Phys. Rev. B 54 (1996) 11796–11802.
- [40] M.O.M. Piepenbrock, T. Stirner, M. O'Neill, S.M. Kelly, Growth dynamics of CdTe nanoparticles in liquid and crystalline phases, J. Am. Chem. Soc. 129 (2007) 7674–7679.